Review Article

Jean Decobert*, Guillaume Binet, Alvaro D.B. Maia, Pierre-Yves Lagrée and Christophe Kazmierski

AlGaInAs MOVPE selective area growth for photonic integrated circuits

Abstract: We developed a generic photonic integration platform based on selective area growth (SAG) by metal organic vapor-phase epitaxy (MOVPE) of AlGaInAs/InP multiple quantum well (MQW) material. For efficient and predictive band gap engineering of photonic integrated circuits, different SAG zones of active and passive function heterostructures are precisely modeled and characterized. With the vapor-phase diffusion model, using numerical simulations of finite volumes, we extracted the three effective diffusion lengths of Al, Ga, and In species. In our growth conditions, these lengths were 32, 65, and 14 μm, respectively. The Kardar-Parisi-Zhang (KPZ) equation, a classic approach to describe the growing interface profile, is used. AlGaInAs MQW properties are then simulated in terms of thickness, composition, band gap, and biaxial strain variations. Highly resolved μ-photoluminescence and optical interferometer microscopy measurements confirm the validity of the band gap and thickness variations for both bulk and MQW layers. A new diffractometer, with a submillimeter X-ray spot, was used to study the structural properties of the MQW in the center of the SAG area. As an application, we present the realization and operation of full-monolithic high-speed advanced modulation format transmitters based on novel prefixed optical phase switching by fast electro-absorption modulators.

***Corresponding author: Jean Decobert,** III–V Lab, Route de Nozay, F-91461 Marcoussis, France, e-mail: jean.decobert@3-5lab.fr
Guillaume Binet: III–V Lab, Route de Nozay, F-91461 Marcoussis, France; and Sorbonne Universités, UPMC Univ Paris 06, CNRS, UMR 7190, Institut Jean le Rond d'Alembert, F-75005 Paris, France
Alvaro D.B. Maia: Pontifícia Universidade Católica, Rua Marquês de São Vicente 225, Rio de Janeiro, 22453-900 Brazil; and Sorbonne Universités, UPMC Univ Paris 06, CNRS, UMR 7190, Institut Jean le Rond d'Alembert, F-75005 Paris, France
Pierre-Yves Lagrée: Sorbonne Universités, UPMC Université Paris 06, CNRS, UMR 7190, Institut Jean le Rond d'Alembert, F-75005 Paris, France
Christophe Kazmierski: III–V Lab, Route de Nozay, F-91461 Marcoussis, France

www.degruyter.com/aot

Keywords: AlGaInAs multiple quantum wells (MQW); electro-absorption modulators; metal organic vapor-phase epitaxy (MOVPE); phase shift keying (PSK); photonic integrated circuit (PIC); selective area growth (SAG).

DOI 10.1515/aot-2015-0013
Received January 19, 2015; accepted February 20, 2015; previously published online March 26, 2015

1 Introduction

The demand for telecommunication speed and capacity continues to grow exponentially, becoming an important enabler of the modern economy. To support this growth, an evolutionary path resulting from simply scaling the existing equipment technologies will not provide an appropriate solution. Great progress has been recently attained by advanced modulation formats and coherent detection. However, their technology or large number of channels inevitably produces highly complex photonic transmitters and receivers having typically an increased footprint, energy, and material consumption, leading in turn to higher fabrication costs. To solve these issues, typical of discrete components, the next break-through will have to rely on highly extensive integration. Providing higher speed and throughput and limiting the footprint and consumption, photonic integrated circuits (PICs) are actually gaining more commercial importance in the optoelectronics industry. Among the few photonic integration technologies (co-package, common hybridization platforms, or common processing hybridization), the full-monolithic approach is certainly the most promising, due to its ease in designing and its reduced footprint and cost. At telecommunication wavelengths, indium phosphide (InP) is the unique material providing the possibility to grow and integrating on a single chip all the required active and passive photonic functions. To simplify the component fabrication and target its high yield,

we developed an integration platform relying on SAG for band gap engineering of AlGaInAs MQWs.

Selective growth has been studied for about 30 years [1, 2]. This technique continues to attract considerable interest as a powerful tool for monolithic integration of active and passive photonic functions. Since the earliest works, considerable efforts have been made to analyze the experimental data, to model the growth mechanisms [3–14], and finally, to serve more and more complex integration schemes, mostly developed for the telecommunication needs [14–17].

SAG by MOVPE is based on the use of structured substrates, where the semiconductor surface is partially covered with dielectric masks. At growth temperature, the atoms provided during the cracking of the active precursors cannot be adsorbed on the amorphous material, leading to the so-called selectivity. They diffuse in the vapor phase and on the mask surface to finally deposit near these dielectric masks, thereby creating localized overgrowth. By a specific optimization of the sizes and shapes of the masks, one can finely adjust the thicknesses (and compositions) of the alloys deposited in any point of the substrate. This approach is particularly effective for MQW structures where electronic transitions mainly depend on well thickness. The more classical design includes two stripes on both sides of the area of interest, holding waveguides and different heterostructures. It is therefore possible to define, on the same wafer and in a single epitaxial step, materials with different energy band gaps, which considerably simplifies the manufacturing processes. Moreover, due to the different decomposition and diffusion rates of the group III precursors in the vapor phase, ternary or quaternary alloys show spatial compositional shift. This shift produces a minor but significant composition-related band gap variation around the mask that cannot be neglected.

In optoelectronics for telecommunication at 1.3 and 1.55 μm, with or without SAG assistance, most of the work has been done on the conventional InGaAsP quaternary material system. As a consequence, the SAG literature is mostly devoted to this material, including the InGaAs ternary alloy. The AlGaInAs quaternary system has, however, demonstrated its high potential as an alternative to InGaAsP and has an increasing industrial impact on the last generation of low-cost telecommunication components. This is due to its larger conduction band gap offset, resulting in higher electron confinement in the quantum wells, which leads to improved gain, characteristic T_0 temperature, and dynamic characteristics of the components. The AlGaInAs quaternary system offers some advantages to control all the different heterostructure compositions needed on InP substrates. Indeed, the layer strain is mostly controlled by the indium mole fraction, whereas the band gap wavelength can be easily adjusted by controlling the Al/Ga ratio. Furthermore, having only one V element, arsenic in this study, leads to abrupt interfaces, contrary to the GaInAsP system where As-P intermixing must be taken into account.

SAG has been widely used for longitudinal integration, in the optical waveguide direction, of active components such as lasers, electro-absorption modulators (EAMs), semiconductor optical amplifiers (SOAs), together with passive sections such as spot size converters (SSCs) [17, 18]. SAG has also demonstrated its high potential for parallel integration, with large wavelength shift of numerous juxtaposed devices such as laser arrays with a passive multimode interference (MMI) coupler, for coarse-wavelength division multiplexing (CWDM) [19, 20]. Transmitters for spectrally efficient modulation formats are excellent candidates for monolithic integration as they need many passive and active functions. With axial and parallel integration modes, SAG has the advantage of a single epitaxial step for all photonic function core materials regardless of the number of required gaps. Other known integration methods such as the butt joint technique may offer the advantage of independent material optimization for two, rarely more, different areas. However, if more than two gaps were needed for optimized photonic functions, multiple butt joints (i.e., multiple regrowths) would be necessary, making this technique too complex for a high fabrication yield. The intermixing technique also has the same limitation since the gap variation is obtained at the price of interface sharpness quantum well quality degradation. Finally, unlike the butt joint technique, where optical reflections occur at each etched and regrown interface, SAG provides genuinely continuous waveguides and ensures the highest-quality MQW core materials with sharp layer interfaces. Relying on SAG gap engineering of AlGaInAs MQW, our integration platform is completed by a semi-insulating buried heterostructure (SIBH) to achieve high-speed modulators, low-loss waveguides, and low thermal resistance [14]. All passive waveguides are unmasked during SIBH regrowth and therefore are naturally covered by iron-doped semi-insulating InP, avoiding high optical losses of p-type cladding, for example, in standard ridge-waveguide integration platforms. A typical linear loss of 14 dB/cm has been experimentally found, allowing to further estimate the overall loss excess of complex integrated circuits according to their size.

In this article, which focusses on the AlGaInAs/InP-based material system, we will describe how the two pillars of SAG, namely modeling and characterization, provide a powerful ‘toolbox’ for band gap engineering and device

designing. As a demonstration, we will present a record of a 224-Gb/s operation of a two-arm ASK-PSK transmitter and report on the realization of likely most complex single-channel QPSK InP-PIC transmitters integrating up to 40 photonic functions.

2 SAG and characterization

During AlGaInAs material growth, the three Al, Ga, and In precursors provide different vapor and surface decomposition rates, leading to different diffusion coefficients in the vapor phase. However, in conventional MOVPE, any desired AlGaInAs composition can be obtained easily by an adjustment of the precursor flow. However, in selective growth, as the precursors cannot deposit on the mask, extra material is available over the masked zone and a lateral concentration gradient builds up. As a result, in the SAG regime, diffusion lengths of Al, Ga, and In precursors become measurable. This is especially important with ternary and quaternary materials, for which spatial compositional variation occurs around the mask. MOVPE SAG can be categorized into wide-stripe SAG (with mask openings >5 μm) and narrow-stripe SAG (with mask opening around 1 or 2 μm). In narrow-stripe SAG, the ridge waveguide laser is directly formed in the narrow opening space between the masks, without any mesa etching step [19, 21]. The difficulty is the growth control near the mask edge due to non-deterministic, surface diffusion influence, which may depend on mask fabrication and processing step history. With a wide-stripe SAG, surface effects can be neglected and the transport of elements is due to their deterministic vapor-phase diffusion (VPD) and InP sticking constants for given growth conditions. In this case, the ridge is formed through standard mesa etching processes in the center region of the mask opening area. The advantage is the 'natural' integration of the passive waveguide region, such as a multimode interference coupler, with the laser array active region. In our study, all the AlGaInAs layers were grown at 680°C and at 150 mbar in an AIX200/4 MOVPE system by wide-stripe SAG [13, 14, 18, 20]. Trimethylaluminum, trimethylgallium, trimethylindium, arsine, and phosphine were the source materials. Purified hydrogen was used as a carrier gas. SAG is extremely growth-condition dependent, the main parameters being growth pressure and growth temperature. To a lesser extent, growth rate and V/III gas flow ratio also affect the growth rate enhancement (GRE) ratio. Nevertheless, these parameters can be easily calibrated in any kind of reactor design. Indeed, the indium and gallium diffusion lengths values obtained in our reactor, as a function of pressure or temperature, are in qualitative agreement with those already reported in the literature from other epitaxial tools in selective growth conditions. The transferability from one reactor to another can be obtained through the fine-tuning of the growth conditions. The main limitation could be the reactor itself and how the best material quality and layer uniformity are compatible with the targeted SAG conditions.

The silica mask stripes were obtained using plasma-enhanced chemical vapor deposition followed by conventional photolithography and reactive ion etching. Usually, the SAG area is surrounded by two parallel dielectric stripes aligned along the [110] crystallographic direction. The cell geometry (Figure 1) is defined by the stripe width *Wm*, the opening width *Wo*, and the stripe length *L*. This design can be reproduced periodically from cell to cell, with *Wx* and *Wy* being the cell width and length, respectively. The SiO_2 dielectric mask led to a perfect selectivity (i.e., no polycrystalline deposition on the mask). The selectivity is mandatory in this process as any undesired material deposition on the dielectric would be lost for the process area and would lead to unpredictable alloy compositions.

Basic material calibrations of thicknesses and compositions are often routinely and rapidly achievable in the laboratories, respectively, by surface profiling and by the association of both photoluminescence and high-resolution X-ray diffraction (HRXRD). Assuming sufficient material uniformity, one measurement is representative of the whole wafer's surface. In SAG, these calibration procedures are much more complex. The numerous cell geometries and the gradual variations inherent to the technique imply that a series of thickness measurements

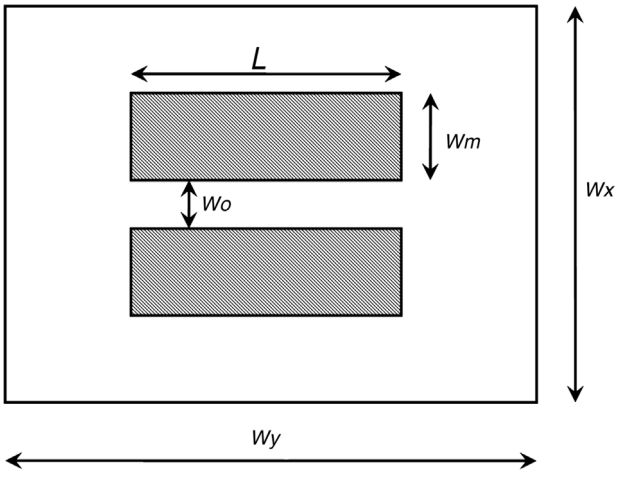

Figure 1: Schematic of the growth pattern with the dimensions *Wm*, *Wo*, *L*, *Wx*, and *Wy*.

must be performed. The oxide mask has to be removed so that the thickness enhancement can be deduced by comparison with the nominal thickness in the 'field' region, far from the mask influence. Optical interferometer microscopy (OIM), a setup from Fogale in our case, should be a preferable technique compared to surface profiling: three-dimensional (3D) thickness cartographies are acquired in few seconds and post-processing allows as many cross sections as required in any direction. The vertical resolution is around ±5 nm (Figure 2). The photoluminescence or micro-photoluminescence (μ-PL) setup should fulfill at least two criteria: the spot size dimensions should be as low as possible (ideally around 1 μm) and the setup should include an optical access to clearly identify the mask cells and to put the laser diode spot into the desired position, generally in between the two mask stripes. Controlled micro-movements are therefore necessary for precise positioning and for wavelength cartography acquisition (Figure 3).

It should be noticed that OIM and μ-PL are basically the only 'home-accessible' and non-destructive characterization tools available. HRXRD is a well-established tool and is definitively the appropriate technique to map multilayer strain and thickness in micro-optoelectronic devices. However, due to the large-incident X-ray beam provided by standard diffractometers (a few millimeters down to half a millimeter), the XRD scans obtained in the laboratory will only give structural information averaged over large areas. To characterize the as-grown layers with submicronic resolution, synchrotron-based X-ray microprobe is the technique of choice [5]. However, due to the limited access to these large facilities, this approach is mainly applicable to specific studies performed on selected samples. Nevertheless, an accurate structural characterization of all daily-grown samples to feedback the growth parameters is highly desirable. That is why an 'in-house' diffractometer is needed but still not efficient for SAG with conventional sources.

Recently, we reported the latest improvements performed in the laboratory with a new high-resolution and small X-ray spot diffractometer on the structural characterization of MQW structures produced by SAG on InP (100) substrates. This setup (D8 Discover from Bruker AXS GmbH, Karlsruhe, Deutschland) is equipped with a microfocus X-ray source (IμS) working at copper $K_{\alpha 1}$ X-ray energy and achieving a submillimeter (50×100 μm^2) spot size on the sample (Figure 4, inset). Accurate lateral positioning of the sample (within 1 μm) is achieved with a laser-video microscope. Even if the X-ray beam spot size remains much larger compared to synchrotron-based microbeam, the area probed here is now at the same scale as the wide-stripe SAG-investigated dimensions. Using this technique, it is possible to access the SAG area between the two mask stripes. From the ω-2θ X-ray profiles, we were able to extract structural information between the mask stripes in the central area. This is possible thanks to a model that we have developed through comparison between the new setup and the synchrotron-based measurements. As shown in Figure 4, the computed profile extracted from the laboratory source is very close to the synchrotron XRD measurement [17].

3 SAG and modeling

A modeling and predictive tool of SAG effects is essential for PIC designing. By 'predictive', we understand here that the simulated band gap values for a given mask pattern are closely corresponding to the actual ones after single

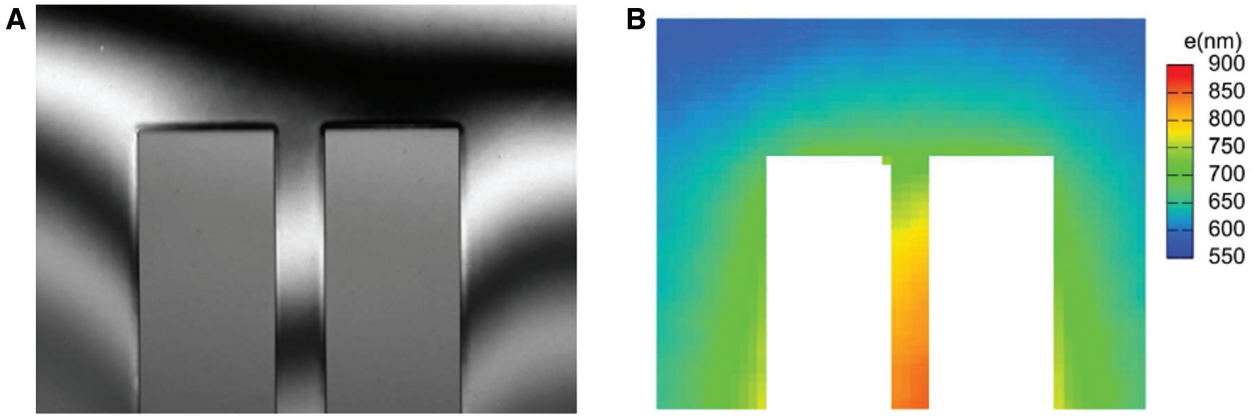

Figure 2: Interferometric thickness measurement: (A) interference fringes and (B) thickness topography.

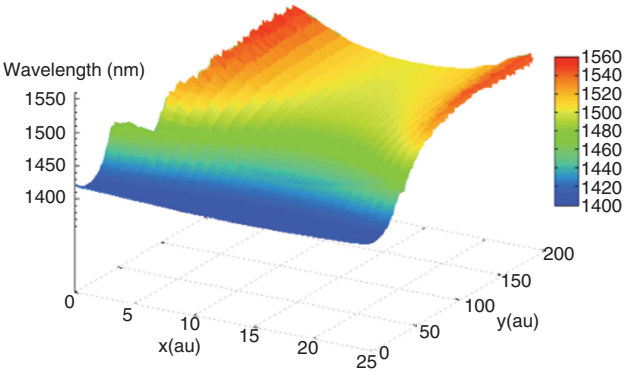

Figure 3: μ-PL cartography of the exit of the SAG region.

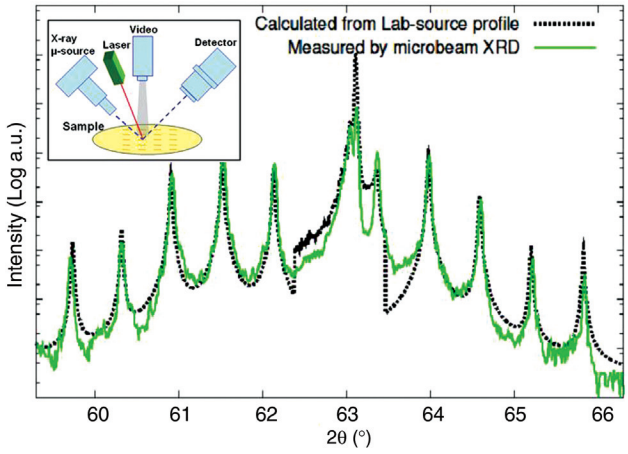

Figure 4: Measured profile (green) using synchrotron radiation compared to extracted profile (black) using a laboratory diffractometer with a submillimeter focused X-ray source and a laser-video microscope (inset).

reference layer stack growth. This is important for industrializing SAG-based components, especially in the case of medium- and large-scale photonic integration in order to avoid expensive design calibrations. We first define each function's heterostructure in the PIC, then we calculate the corresponding mask stripe geometry, and finally, we extract the 'reference' heterostructure that should be effectively grown. That is why a full three-dimensional model that calculates all material parameters, such as composition, strain, or thickness, or the complete layer stack everywhere on the substrate is mandatory in designing the engineered band gaps.

If we consider that the source of material is only supplied through the VPD process, it gives us a simple way to model the SAG regime [5, 6]. This is only possible if the areas of interest are far away from the masks, as in the case of wide-stripe SAG. This approach assumes a laminar flow, the existence of a stagnant layer in contact with the wafer surface, and the absence of deposition on the mask surface. The molecules diffuse and are incorporated onto the exposed crystal surface. Surface diffusion on the mask is ignored in the present model as it occurs within only a few micrometers of the dielectric edge. We solve the Laplace equation of the concentration in three dimensions with specific boundary conditions (Figure 4). Because no species are incorporated on the mask, the flux is equal to 0, which gives us $(\partial N/\partial z)_{z=0}=0$. On the crystal, a combination of the Langmuir isotherm-like condition and the Fick's law $D(\partial N/\partial z)_{z=0}=k_s N$ is considered, with k_s as an adsorption rate constant that depends on the reactivity of source molecules on the crystal surface and D being the diffusion coefficient of the reactants in the vapor phase. Then the concentration is assumed constant $N(H)=N_0$ (i.e., infinite diffusion source) at the top of the stagnant layer. Finally, for left and right boundaries, the periodicity of the domain leads to $(\partial N/\partial x)_{x=Wx/2}=(\partial N/\partial x)_{x=-Wx/2}$ and $N_{x=Wx/2}=N_{x=-Wx/2}$. These boundary conditions are depicted in Figure 5.

A more accurate approach consists in utilizing a modified KPZ equation. In this new calculation, we take into account different phenomena that modify the profile: the overgrowing material at the edge of the mask, the surface migration on the mask, and also the non-trivial relaxation patterns. The KPZ model is well-fitted to this aim and is governed by [22–24]

$$\frac{\partial h(x,t)}{\partial t}=\frac{\lambda}{2}\left(\frac{\partial h(x,t)}{\partial x}\right)^2+\nu\frac{\partial^2 h(x,t)}{\partial x^2}+\xi(x,t) \qquad (1)$$

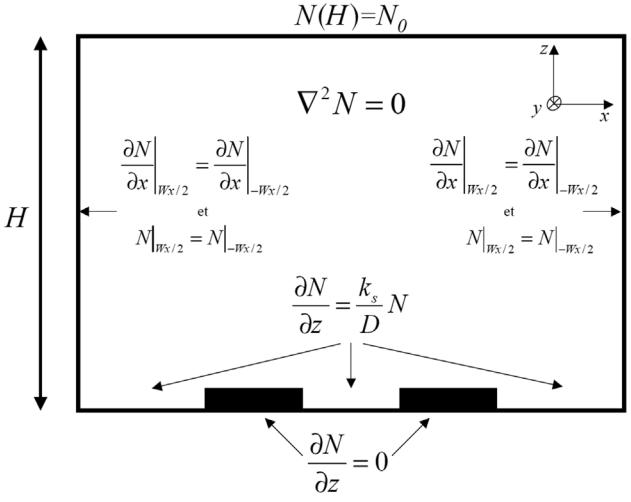

Figure 5: Schematic of the periodic window calculation with governing equations and boundary conditions.

In this equation, $h(x,t)$ is the height of the profile above a horizontal baseline, λ represents the lateral surface growth in a normal direction or the strength of the growth depending on the slope of the surface, v is a diffusion effect, and ξ is a noise contribution. It is an equation describing the temporal growth of interface in the presence of noise, which was originally conceived to describe random deposition and diffusion.

To adapt the KPZ equation to the SAG problem, a new derivation has to be made based on the SAG profile; starting from a Taylor expansion at order 2 [up to $O(h^2)$] of the SAG equations, considering a small h and a small slope dh/dx (Figure 6), we can identify coefficients given by the VPD model

$$\lambda=\frac{\partial N}{\partial y_{y=0}},\quad v_0=\frac{\partial N}{\partial x_{y=0}},\quad \beta=\frac{\partial^2 N}{\partial x\partial y_{y=0}},\quad v_c=\frac{\partial^2 N}{\partial^2 y_{y=0}}.$$

We add a diffusion term that allows for surface diffusion on the mask that was neglected up to now and not taking into account in the noise, this gives a modified KPZ equation:

$$\frac{\partial h}{\partial t}\simeq -v_0\frac{\partial h}{\partial x}+\lambda\left[1-\frac{1}{2}\left(\frac{\partial h}{\partial x}\right)^2\right]+v\frac{\partial^2 h}{\partial x^2}-\beta\left(h\frac{\partial h}{\partial x}\right)+v_c h. \qquad (2)$$

Thus, the simulation is a two-step process where the VPD model is applied to obtain the parameters of Equation 2. By solving this equation, we obtain the profile as a function of time.

Numerical results were obtained using finite volumes. The concentration profile depends not only on the mask dimensions Wm and Wo, but also on the dimensions of the calculation window, Wx and Wy, which define the periodicity of the domain. In the calculation, the cell in Figure 1 is assumed to be surrounded by identical cells with the same dimensions Wx and Wy. These close cells actually play an important role, as they will interfere with each other. This periodicity is fundamental in modeling the SAG process, especially for device integration, where a large number of closely spaced components are usually desired. The main advantage of the VPD approach is to give a simple way to determine the effective diffusion length (D/k_s parameter), which is, apart from the geometrical dimensions of the mask, the only adjustable parameter of the model.

In the case of AlGaInAs alloys, three effective diffusion lengths are considered: $(D/k_s)_{Al}$, $(D/k_s)_{Ga}$, and $(D/k_s)_{In}$. To determine these parameters, we have previously reported the cross-section thickness measurements of AlAs, GaAs, and InAs binary layers deposited by SAG and measured using the OIM setup [14]. A precise adjustment between the calculated and the experimental thickness profiles leads to the D/k_s parameter for each element from group III. To further increase the accuracy of the measurements, mainly in high-cell-density configuration, specific and more complex heterostructures were grown by SAG and characterized synchrotron-based microprobe techniques. Through periodic structures such as InP/InAsP or GaAs/GaAlAs superlattices, thicknesses were precisely measured in predetermined areas.

Figure 7 shows the GRE as a function of mask width Wm for Al, Ga, and In for three different growth pressures (50, 100, and 150 mbar). Dots are experimental results obtained by submicron synchrotron-based XRD in the middle of the opened area (Wo=40 µm). Fitted lines are modeled to extract the D/k parameters. From these results, the three extracted diffusion lengths in our growth conditions are $(D/k_s)_{Al}$=32 µm, $(D/k_s)_{Ga}$=65 µm, and $(D/k_s)_{In}$=14 µm at 150 mbar. The indium and gallium values are in qualitative agreement with those already reported in the literature [4–8]. The aluminum diffusion length is found intermediate between that of indium and that of gallium. This is demonstrated in Figure 7B through the intermediary slope of aluminum GRE for three different growth pressures. Indeed, near the mask, the slope of the AlAs thickness enhancement profile (Figure 6A) appears steeper than the GaAs one (Figure 6B). The extracted D/k_s are key parameters for model refining and accurate prediction of thickness and compositional variations of ternary and quaternary alloys.

4 SAG-based transmitter PICs

Using predictive SAG designing of AlGaInAs MQWs and SAG-SIBH platform, we have fabricated several PICs [14, 18]. In this article, we focus first on full-monolithic transmitters (TX) for advanced modulation formats and based on novel concept of prefixed optical switching by EAMs [24]. EAM switching strongly decreases the PIC footprint,

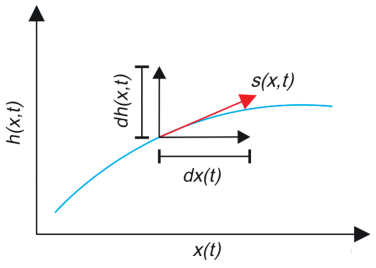

Figure 6: Schematic of the surface parameterization.

allows low-voltage drive, and provides easy speed scaling compared with standard optical phase modulators. The switching principle was shown to produce complex amplitude and phase keying formats and is discussed in detail elsewhere [25–28].

One of the simplest PIC TX architectures is a DFB laser and two EAMs in interferometric push-pull arrangement. This circuit is of very similar complexity as the popular electro-absorption modulated laser (EML) and therefore might achieve similar low-cost targets. Five active (one DFB laser, two phase shifters, and two EAMs) and four passive functions (passive waveguide, one MMI 1:2, one MMI 2:1, and SSC taper) were integrated with SAG using three different material gaps [26]. Figure 8 shows a simulated energy gap along the circuit waveguides together with an actual PIC photograph. Microphotoluminescence measurement confirmed the three designed values of gap wavelengths in the reference, laser, and modulator areas.

To check the correct operation of the circuit, we tested first the two-arm interferometer using the integrated DFB emitter and phase shifters. As shown in Figure 9, the phase

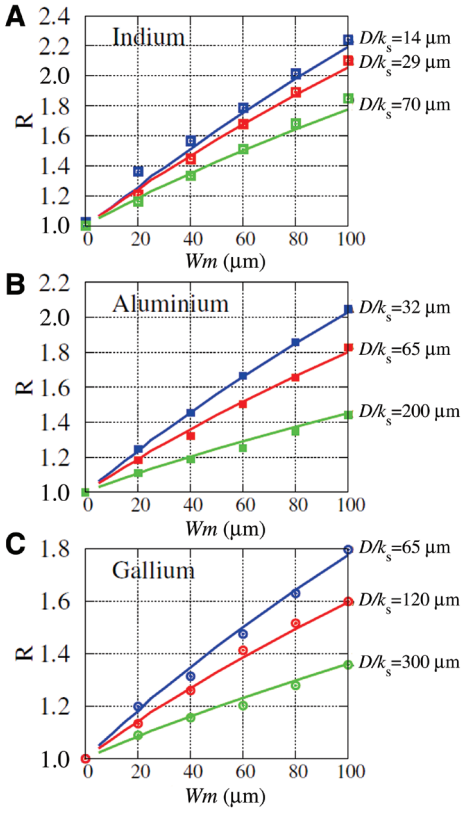

Figure 7: GRE ratio (*R*) as a function of mask width, *Wm*, for indium (A), aluminum (B), and gallium (C) for three different growth pressures (blue, 150 mbar; red, 100 mbar; green, 50 mbar). Dots are experimental results obtained by synchrotron-based XRD and fitted lines are modeled to extract the *D*/*k* parameters.

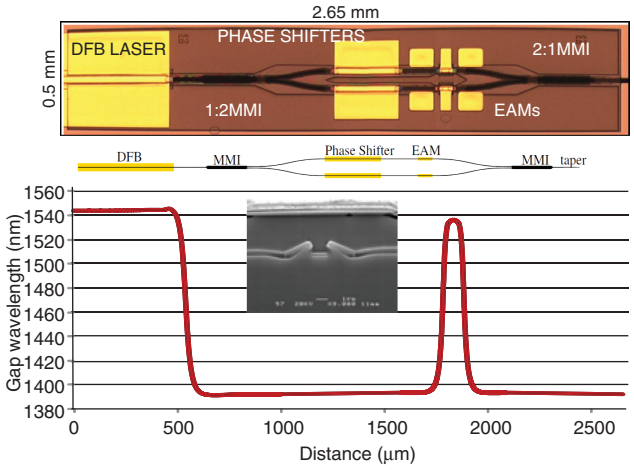

Figure 8: SAG design of photoluminescence wavelength for each photonic function area of the two-arm transmitter shown with the circuit architecture schematic and an actual chip photograph. The inset photograph reminds the device lateral cross section in the active areas showing our SIBH regrowth surrounding MQW waveguide core.

shifters provided large optical phase variations, leading to constructive and destructive interferences at the PIC output. The measured interference extinction ratio was >20 dB, confirming correct phase control and good power balance in the arms. As a next step, we checked the switching ability of EAMs. Figure 10 shows the power-voltage characteristics for 50-µm-long EAMs leading to a switching extinction ratio up to 18 dB. Measured EAM modulation bandwidth was above 20 GHz [26]. All circuit provided an output power of +2 dBm CW and -5 dBm when modulated.

We rely on a two-arm interferometric structure to modulate light along the positive and negative parts of a single axis (e.g., the real axis) in the complex plane. To do so, we first assigned a phase difference of π between the

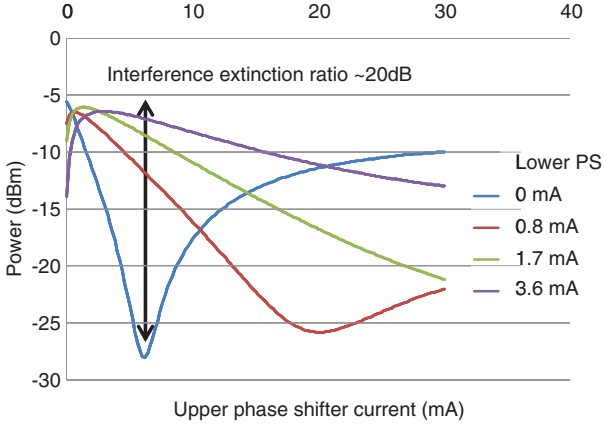

Figure 9: PIC output power measures for different phase shifter bias showing constructive and destructive interferences.

two arms of the interferometer by adjusting the current of the PSs. In the most advanced multilevel experiments [27], we derived the EAMs with complementary electrical waveforms, supplied by digital-to-analog converter of 8-bit resolution, followed by linear amplifiers-drivers delivering 3 V peak-to-peak with 32 GHz bandwidth. We engineer the waveforms such that they can alternatively take any of the four equally spaced voltage levels, instead of two levels, so that the resulting optical signal carries twice as much bit rate at unchanged symbol rate. Hence, after splitting and recombining via the MMI couplers, light from the DFB laser carries data with two-level amplitude shift keying (2ASK) and two-level phase shift keying (2PSK), as depicted in the measured constellation of Figure 11.

Using this modulation format 2ASK-2PSK, we put our chip in a noise-loaded system bed and measured transmission Q^2 factor vs. optical signal-to-noise ratio (OSNR) in a 0.1-nm spectral band for different baud rates 16, 28, 40, and 56 GBaud. The results are represented in Figure 12 vs. theoretical required OSNR for the format. All experiments are done with orthogonal polarization diversity emulation multiplying the data rate by 2 in the fiber line and at the receiver. Error-free operation with soft-decision forward error correction (20% overhead) was possible up to 56 GBaud corresponding to 224 Gb/s. This result established a new speed record for BPSK-related formats due to fast EAM switches. Error floors are observed for all baud rates giving 2–4 dB OSNR margin above SD-FEC level, emphasizing that the improvements are required for the source-modulated power and dynamic extinction ratio. Simultaneously, very low OSNR penalties, compared with theory, are observed up to 40 GBaud, likely limited by the PIC assembly bandwidth. This result confirms the pertinence of the proposed novel transmitter concept vs. established phase modulators.

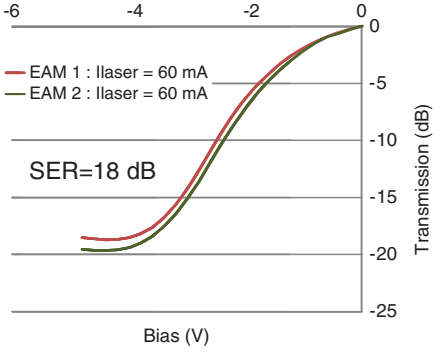

Figure 10: Transfer characteristics (transmitted power-voltage) of our 50-µm-long EAMs showing up to 18 dB of switching extinction ratio.

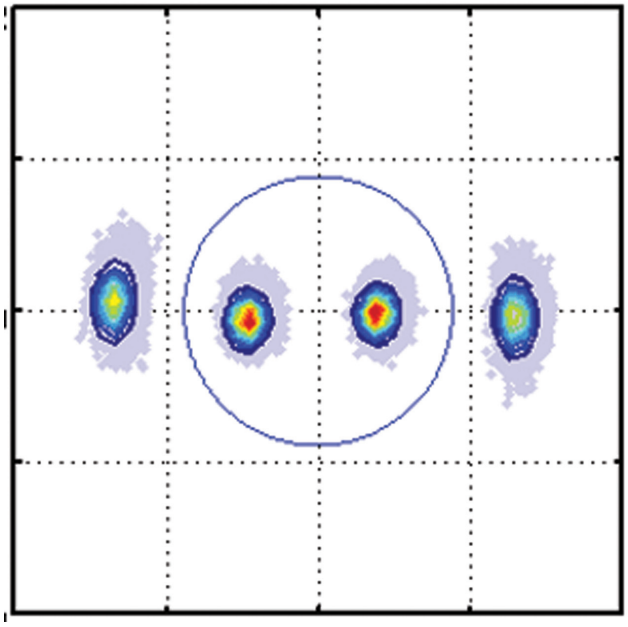

Figure 11: Measured constellation of 2ASK-2PSK modulation at 28 GBaud (56 Gb/s) in the complex amplitude/phase space.

The two-arm PIC dimensions are 2.65×0.5 mm, making it the smallest reported over 100-Gb/s-capable integrated transmitter for advanced format modulations, to the best of our knowledge. Such a low size enables usage of the lowest-form factor packages (including TO-can), which is the most important key to lower the transmitter costs.

More recently, we pushed forward the integration complexity using the described SAG platform and realized

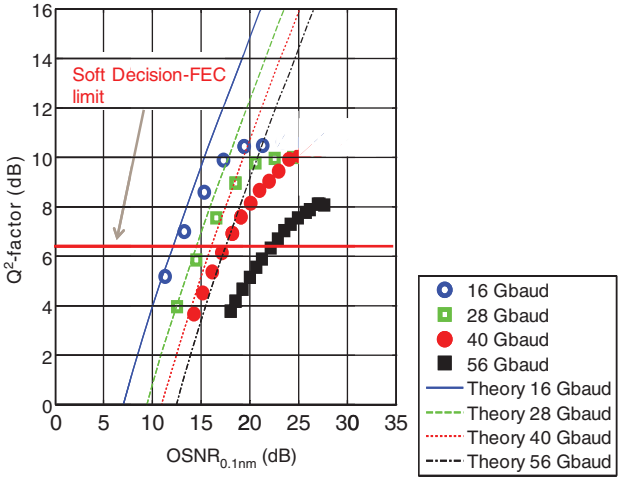

Figure 12: Q^2 factor vs. OSNR characteristics measured (dots) in a noise-loaded transmission system for different baud rates and compared with theoretical ones (lines). Error-free operation with soft-decision FEC was possible up to 56 Gbaud. Very low OSNR penalties vs. theory are observed up to 40 Gbaud [28].

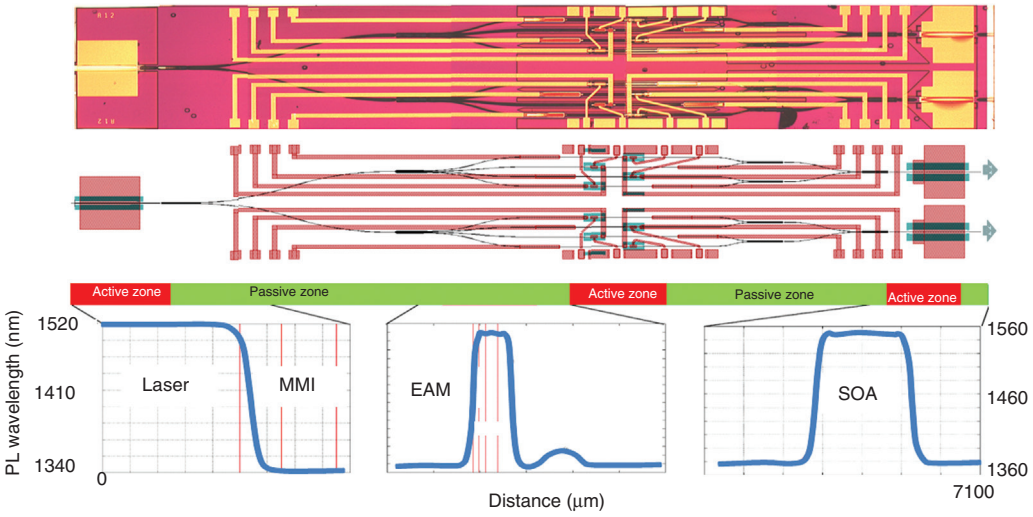

Figure 13: Gap wavelength variation realized by SAG shown together with polarization diversity full-monolithic QPSK transmitter schematics and actual chip photograph.

a 2×4-arm transmitter, including polarization diversity (PDM) capability implemented via two outputs for external polarization management. This circuit includes one DFB laser, eight phase shifters, eight variable optical attenuators (VOA), eight EAM switches, two SOAs, two MMI 1:4, seven MMI 2:1, two SSC tapers, and waveguide connectors. This circuit includes two SOAs for 10-dB linear transmission loss compensation. Owing to the optimized operation of each active function, up to five different energy gaps had to be simulated and realized with SAG (laser, EAM, VOA, SOA, and 'reference'for phase shifters and all passive functions). It would be difficult to imagine a different technology other than SAG to optimize the number of gaps with high QW layer quality and without spurious reflections between different components. Simulated (and actual) gap wavelength variations are reported as a function of device length on Figure 13, together with the corresponding PIC areas [28]. A two-channel schematic is shown together with actual circuit photographs with all integrated functions.

With its 38 integrated photonic functions, the chip is probably the most complex monolithic single-channel InP PIC. All functions were operational, with characteristics similar to the simpler two-arm circuit. The circuit size is 7.1×1 mm, which is currently the smallest PDM-QPSK transmitter, whatever the technology used.

Although the proposed TX integration on InP based on SAG of AlGaInAs MQW and SIBH has yet to gain maturity and fully exploit its improvement potential, we believe that this kind of very compact PIC can actually allow migration of spectrally efficient vector modulation formats toward terminal-cost-sensitive networks such as metropolitan, access, or datacom.

5 Conclusion

SAG has been extensively employed for the fabrication and integration of a wide range of InP-based optoelectronic devices. As an alternative to the InGaAsP material system, AlGaInAs is of considerable interest in improving the thermal and dynamic characteristics of the devices. We studied the SAG modeling and characterization of the AlGaInAs material system. We used a 3D VPD model to extract the effective diffusion lengths of Al, Ga, and In species from measured thickness profiles of the three binaries, AlAs, GaAs, and InP. Our growth conditions yield 32 μm, 65, and 14 μm for Al, Ga, and In, respectively. Based on these values, we achieved a precise prediction of AlGaInAs thickness, composition, band gap, and biaxial strain variations. In the case of high mask density, particular attention was paid to interferences between neighboring cells due to the long-range effect of aluminum and gallium species. High-resolution μ-PL and OIM measurements confirmed the validity of simulated band gap and thickness variations for both bulk and MQW layers. We have also shown that well-targeted structural information can be extracted from the SAG area with a laboratory diffractometer equipped with a submillimeter (down to 100 μm and lower) X-ray source. The VPD model is able to predict with a high accuracy the SAG effects for

any AlGaInAs structure, including complex stacking like MQW layers. This offers a very attractive tool for complex and precise engineering of SAG optoelectronic integrated devices. As an application, we present the realization and operation of full-monolithic high-speed advanced modulation format transmitters based on novel prefixed optical phase switching by fast EAM. We have obtained a record 224-Gb/s operation of a two-arm ASK-PSK transmitter and report on the realization of likely most complex single-channel QPSK InP-PIC transmitters integrating up to 40 photonic functions.

Acknowledgments: This work has received partial financial support from the IST-MIRTHE project. The authors acknowledge the contributions of Guilhem de Valicourt, Haïk Mardoyan, Katarzyna Ławniczuk, and Nicolas Chimot.

References

[1] J. P. Duchemin, M. Bonnet, F. Koelsch and D. Huyghe, J. Cryst. Growth 45, 181 (1978).
[2] R. Azoulay, N. Bouadma, J. C. Bouley and L. Dugrand, J. Cryst. Growth 55, 229 (1981).
[3] R. Bhat, J. Cryst. Growth 120, 362 (1992).
[4] C. Caneau, R. Bhat, C. C. Chang, K. Kash and M. A. Koza, J. Cryst. Growth 132, 364 (1993).
[5] M. Gibbon, J. P. Stagg, C. G. Cureton, E. J. Thrush, C. J. Jones, et al., Semicond. Sci. Technol. 8, 998 (1993).
[6] T. Fujii, M. Ekawa and S. Yamazaki, J. Cryst. Growth 156, 59 (1995).
[7] A. Ougazzaden, L. Silvestre, A. Mircea, N. Bouadma, G. Patriarche, et al., in 'IPRM Proceedings' (1997).
[8] M. A. Alam, R. People, E. Isaacs, C. Y. Kim, K. Evans-Lutterodt, et al., Appl. Phys. Lett. 74, 18 (1999).
[9] H. Oh, M. Sugiyama, Y. Nakano and Y. Shimogaki, Jpn. J. Phys. 42, Pt. 1, 6284 (2003).
[10] M. Sugiyama, H. Oh, Y. Nakano and Y. Shimogaki, J. Cryst. Growth 261, 279 (2004).
[11] F. Ollson, T. Zhu, G. Mion and S. Lourdudoss, J. Cryst. Growth 289, 24 (2006).
[12] T. Shioda, M. Sugiyama and Y. Nakano, in 'IPRM Proceedings', 43 (2007).
[13] J. Décobert, N. Dupuis, P. Y. Lagrée, N. Lagay, A. Ramdane, et al., J. Cryst. Growth 298, 28 (2007).
[14] N. Dupuis, J. Decobert, P.-Y. Lagrée, N. Lagay, F. Poingt et al., J. Appl. Phys. 103, 113113 (2008).
[15] D. Delprat, A. Ramdane, L. Silvestre, A. Ougazzaden, F. Delorme, et al., IEEE Photon. Tech. Lett. 9, 7 (1997).
[16] G. Laube, IPRM Proc. 392 (1996).
[17] B. Mason, S. Chandrasekhar, A. Ougazzaden, C. Lentz, J. M. Geary, et al., IEEE Photon. Tech. Lett. 14, 1 (2002).
[18] N. Dupuis, J. Decobert, C. Jany, F. Alexandre, A. Garreau, et al., IEEE Photon. Tech. Lett. 20, 2 (2008).
[19] T. Sasaki and K. Kudo, in 'WDM Technologies' (Academic Press, 2002).
[20] J. Décobert, N. Dupuis, P. Y. Lagrée and N. Lagay, in 'IPRM Proceedings' (2008).
[21] W. Feng, W. Wang, H. Zhu, L. Zhao, L. Hou, et al., Semicond. Sci. Technol. 20, 1083 (2005).
[22] M. Kardar, G. Parisi and Y. Zhang, Phys. Rev. Lett. 56, 889 (1986).
[23] M. T. Batchelor, R. V. Burne, B. I. Henry and S. D. Watt, Physica A 282, 123–136 (2000).
[24] T. Gueudré, P. Le Doussal, A. Rosso, A Henry and P. Calabrese, Phys. Rev. E 86, 041151 (2012).
[25] I. Kang, in 'OFC Proceedings' (2006).
[26] C. Kazmierski, N. Chimot, F. Jorge, A. Konczykowska, F. Blache, et al., in 'OFC Proceedings' (2014).
[27] G. de Valicourt, M. A. Mestre, P. Jennevé, H. Mardoyan, J. C. Antona, et al., in 'IPRM Proceedings' (2014).
[28] H. Mardoyan, O. Bertran-Pardo, P. Jennevé, G. de Valicourt, M. A. Mestre et al., in 'OFC Proceedings' (2014).

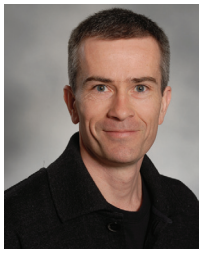

Jean Decobert
III–V Lab, Route de Nozay, F-91461 Marcoussis, France
jean.decobert@3-5lab.fr

Jean Decobert has been working on III-V epitaxial growth by MOVPE since he started his Master's degree in Materials Sciences in 1987. After receiving his PhD in Electronics from the University of Lille in 1993, he joined the National Center of Telecommunication Research (CNET) in France. In 2004, he became a research engineer at the III-V Lab (the joint laboratory founded by Alcatel-Lucent and Thales R&T in 2004 and including CEA-Leti since 2011), where he is currently in charge of III-V active material growth by MOVPE for opto-electronic applications. His research activities mainly involve advanced Electroabsorbtion Modulator-Lasers (EML), Avalanche Photo-Diodes (APD) for Photonic Integrated Circuits (PIC), and p-i-n photodiodes for SWIR imaging. Actually, he is currently working on the Selective Area Growth (SAG) technique, the advanced technology platform for optoelectronic device integration.

Guillaume Binet
III–V Lab, Route de Nozay, F-91461 Marcoussis, France; and Sorbonne Universités, UPMC Univ Paris 06, CNRS, UMR 7190, Institut Jean le Rond d'Alembert, F-75005 Paris, France

Guillaume Binet was born in Paris, France on March 23, 1990. He received the MS in optoelectronics in 2013 from the Grenoble Institute of Technology and the MA in innovation and entrepreneurship from the Institute of Political Studies in Grenoble in 2014. He is currently working toward a PhD at the III-V lab in Marcoussis and the Pierre and Marie Curie University in Paris, focused on the development of photonic integrated circuits (PIC) by selective area growth (SAG) for optical telecommunications in the 1.3 μm band.

Alvaro D. B. Maia
Pontifícia Universidade Católica, Rua Marquês de São Vicente 225, Rio de Janeiro, 22453-900 Brazil; and Sorbonne Universités, UPMC Univ Paris 06, CNRS, UMR 7190, Institut Jean le Rond d'Alembert, F-75005 Paris, France

Alvaro Diego Bernardino Maia was graduated in Physics University of Brasilia (2005, Brazil) and received the master's degree in Physics from the University of São Paulo (2007, Brazil) and PhD from the University of São Paulo (2012, Brazil). He has experience in physics of semiconductor materials, growth and processing of semiconductor devices. His research interests include simulations and theoretical modeling of physical and electronic processes in quantum heterostructures.

Pierre-Yves Lagrée
Sorbonne Universités, UPMC Université Paris 06, CNRS, UMR 7190, Institut Jean le Rond d'Alembert, F-75005 Paris, France

Pierre-Yves Lagrée was born in Courrières, France, in 1965. He joined Ecole Normale Supérieure Saint-Cloud/Lyon in 1985, and obtained the Agrégation de Physique in 1988. He stayed one year at ONERA. He received the PhD degree in fluid mechanics in 1992 and HDR in 2006 from University Paris 6. Currently, he is Senior Scientist in CNRS at the Institute Jean le Rond d'Alembert Paris 6, France. His research interests include asymptotic methods, biomechanics, granular flows and fluid mechanics.

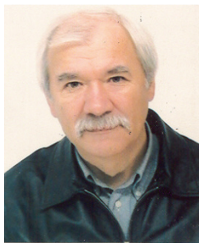

Christophe Kazmierski
III–V Lab, Route de Nozay, F-91461 Marcoussis, France

Christophe Kazmierski was born 1950 in Gdansk, Poland. In early eighties, he contributed to pioneering work on long-wavelength lasers at the Central Research Laboratory of Thomson-CSF. From 1993 to 1999 he also headed the Laser Department of France Telecom R&D CNET, working on laser-based photonic circuits. In 1999 he has been engaged in OPTO+, joined research laboratory between France Telecom and Alcatel Corporate Research Center where he took Group Leader position working on hyper-frequency optical conversion and high speed lasers. In 2001 he left FT R&D and continued as Group Leader in Alcatel R&I. In 2004 this activity has been included in joined laboratory Alcatel-Thales III-V Lab. Presently, his personal research is focused on 10–1000Gbps electro-absorption modulator-based Photonic-Integrated-Circuit sources. He has authored over 300 papers and 18 patents in the field of III-V semiconductors. He has also served on program committees at International Semiconductor Laser, Microwave Photonics and Indium Phosphide and Related Materials Conferences. He has been involved as responsible in a dozen of co-operative international ESPRIT263, RACE I, RACE II, EUREKA, IST and national ANR, RNRT programs. Recently he led the ANR-ANTARES project and IST-MIRTHE project.